Article

Neuron

Origins of Cell-Type-Specific Olfactory Processing in the *Drosophila* Mushroom Body Circuit

Highlights

- Three types of KCs integrate synaptic excitation similarly but spike differently
- KCs receive local, lateral inhibition via APL neurons depending on input strength
- α'/β' KCs recruit feedback inhibition mediated by APL neurons most effectively
- α'/β' KCs have the highest odor detection speed, sensitivity, and discriminability

Authors

Kengo Inada, Yoshiko Tsuchimoto, Hokto Kazama

Correspondence

hokto_kazama@brain.riken.jp

In Brief

Inada et al. discover that principal neurons in the *Drosophila* mushroom body generate spikes and recruit feedback inhibition in a cell-type-specific manner. As predicted from these findings, they further demonstrate that different cell types have distinct odor detectability and discriminability.

Inada et al., 2017, Neuron *95*, 357–367
July 19, 2017
http://dx.doi.org/10.1016/j.neuron.2017.06.039

CellPress

Neuron
Article

Origins of Cell-Type-Specific Olfactory Processing in the *Drosophila* Mushroom Body Circuit

Kengo Inada,[1,3] Yoshiko Tsuchimoto,[1] and Hokto Kazama[1,2,3,4,*]
[1]RIKEN Brain Science Institute, 2-1 Hirosawa, Wako, Saitama, 351-0198, Japan
[2]RIKEN BSI-KAO Collaboration Center, 2-1 Hirosawa, Wako, Saitama, 351-0198, Japan
[3]Graduate School of Arts and Sciences, The University of Tokyo, 3-8-1 Komaba, Meguro-ku, Tokyo, 153-8902, Japan
[4]Lead Contact
*Correspondence: hokto_kazama@brain.riken.jp
http://dx.doi.org/10.1016/j.neuron.2017.06.039

SUMMARY

How cell-type-specific physiological properties shape neuronal functions in a circuit remains poorly understood. We addressed this issue in the *Drosophila* mushroom body (MB), a higher olfactory circuit, where neurons belonging to distinct glomeruli in the antennal lobe feed excitation to three types of intrinsic neurons, α/β, α′/β′, and γ Kenyon cells (KCs). Two-photon optogenetics and intracellular recording revealed that whereas glomerular inputs add similarly in all KCs, spikes were generated most readily in α′/β′ KCs. This cell type was also the most competent in recruiting GABAergic inhibition fed back by anterior paired lateral neuron, which responded to odors either locally within a lobe or globally across all lobes depending on the strength of stimuli. Notably, as predicted from these physiological properties, α′/β′ KCs had the highest odor detection speed, sensitivity, and discriminability. This enhanced discrimination required proper GABAergic inhibition. These results link cell-type-specific mechanisms and functions in the MB circuit.

INTRODUCTION

Neural circuits organize diverse types of cells to exert specific functions. Examining how each type of cell behaves in a circuit is therefore central to understanding the basis of neural processing. In the cerebral cortex comprising highly heterogeneous cells, neurons have been typically characterized and classified based on the morphological, molecular, and physiological features (Ascoli et al., 2008), an effort that continues at an increasingly comprehensive scale (Markram et al., 2015; Tasic et al., 2016). The major challenge following the characterization of cell-intrinsic properties is two-fold. First is to examine synaptic interactions between these cells. Second is to examine how intrinsic and synaptic properties together determine the function of a cell type in the context of specific information processing such as sensory processing.

To address these challenges, here we focused on the *Drosophila* mushroom body (MB), a circuit critical for olfactory association (Heisenberg, 2003). Olfactory information conveyed to the MB is represented by the activity of ~2,000 Kenyon cells (KCs), which can be classified into α/β, α′/β′, and γ types from morphological and developmental characteristics (Aso et al., 2009; Crittenden et al., 1998; Lee et al., 1999). The axons of these three types of KCs form α/β, α′/β′, and γ lobes of the MB, respectively. Different types of KCs show spontaneous and odor-evoked spikes with distinct characteristics (Turner et al., 2008). Moreover, genetic manipulations of KCs have suggested that olfactory memory is engraved in multiple lobes and specific sets of them are necessary for retrieving recent and remote memories (Blum et al., 2009; Cervantes-Sandoval et al., 2013; Krashes et al., 2007; Krashes and Waddell, 2008; Trannoy et al., 2011; Xie et al., 2013). Although these functional differences between lobes indicate that the activity of each KC type must arise through cell-type-specific mechanisms, this has not been physiologically investigated.

KCs receive excitatory drive from projection neurons (PNs; Caron et al., 2013; Gruntman and Turner, 2013), each of which belongs to one of ~51 glomeruli in the antennal lobe, the primary olfactory processing center (Figure 1A; Stocker et al., 1990; Tanaka et al., 2012). Individual KC is connected, on average, to seven PNs randomly (Caron et al., 2013) with some biases (Gruntman and Turner, 2013). KCs are also under a recurrent, inhibitory control of GABAergic anterior paired lateral (APL) neurons (Figure 1A; Lin et al., 2014; Liu and Davis, 2009; Tanaka et al., 2008). A single APL neuron in a hemisphere extends processes throughout the MB. How these excitatory and inhibitory synaptic inputs as well as cell-intrinsic properties interact to shape the output of each KC remains elusive.

In this study, we investigated this question by stimulating individual presynaptic neurons with single- and two-photon optogenetics while monitoring postsynaptic activity in KCs with intracellular recording. Our approach revealed that whereas three types of KCs integrate excitatory inputs similarly, they generate spikes and recruit APL neuron-mediated inhibition in a cell-type-specific manner. Furthermore, recording of KC odor responses found previously uncharacterized functions of α′/β′ KCs in olfactory processing that were predicted from these cell-type-specific properties: more rapid detection of an odor and enhanced discrimination between different odor concentrations.

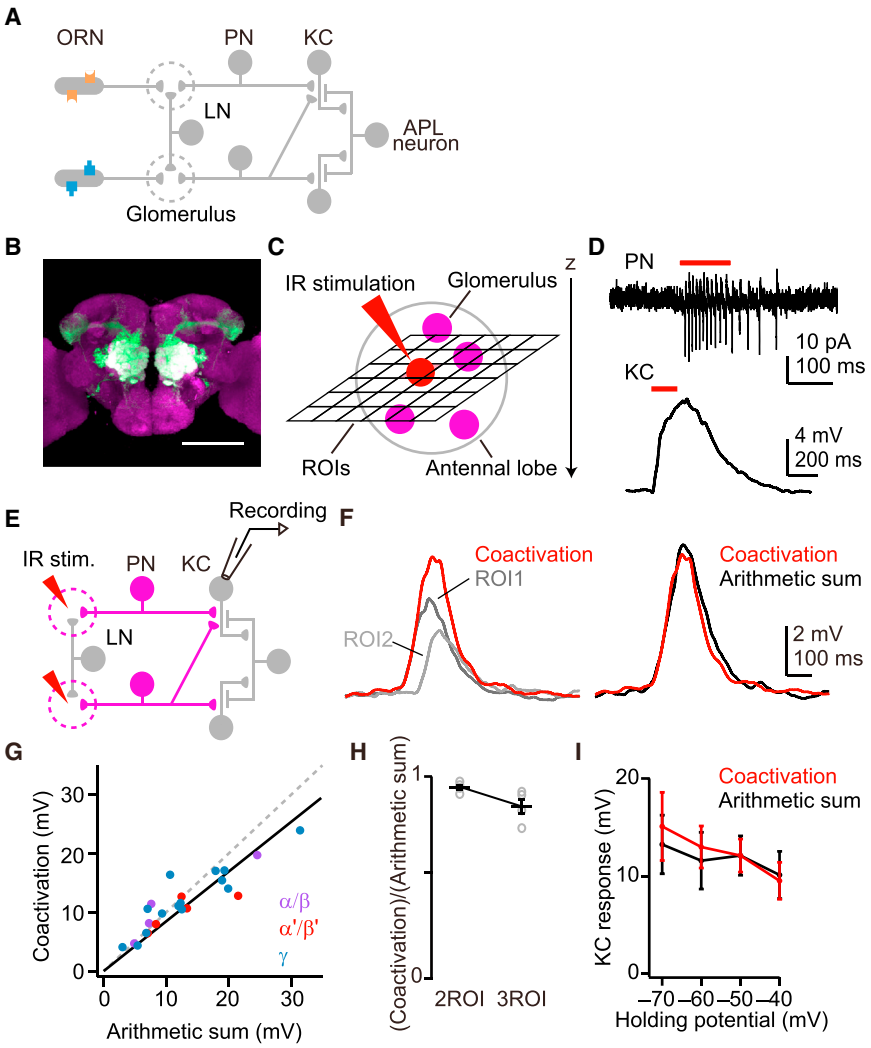

Figure 1. Two-Photon Optogenetics Shows that KCs Combine Inputs from Multiple PNs Linearly

(A) The *Drosophila* olfactory circuit. ORN, olfactory receptor neuron; LN, local neuron; PN, projection neuron; KC, Kenyon cell; APL neuron, anterior paired lateral neuron.

(B) Projection of a confocal stack of a fly brain (neuropil in magenta) expressing myr::GFP (green) driven by *VT33006-Gal4*. *VT33006-Gal4* labels ~44 antennal lobe glomeruli. Scale bar, 100 μm. See Table S1 for the identity of labeled glomeruli.

(C) Schematic of the experiment. ReaChR driven by *VT33006-Gal4* was stimulated by a pulsed infrared (IR) laser. A horizontal plane covering the entire antennal lobe was divided into 6 × 6 ROIs and the IR light was sequentially applied to individual ROIs one at a time. The size of each ROI is 12 μm × 12 μm. The antennal lobe was optically sectioned at 5 μm intervals along the z axis.

(D) Top: sample cell-attached recording of PN spikes in response to IR stimulation (red). Bottom: sample whole-cell recording of a KC response to the same stimulus.

(E) Schematic of the synaptic integration experiment.

(F) Representative KC responses to optogenetic activation of single ROIs (gray traces) and co-activation of these ROIs (red). Black is an arithmetic sum of single ROI responses. Each trace is an average of three trials. Short time difference between individual KC responses reflects the time for the laser to travel from the first to the second ROI (see Figure S2A).

(G) All KC types integrate inputs from multiple PNs approximately linearly (slope = 0.89, 0.75, 0.86 for α/β, α′/β′, and γ KCs, respectively, n = 4, 5, 15 for α/β, α′/β′, and γ KCs, respectively). Black line represents a linear fit for all KCs (slope = 0.85, $R^2 = 0.81$, $p < 10^{-7}$).

(H) KCs add inputs from up to three ROIs approximately linearly (pairwise data, n = 4 KCs).

(I) Response to coactivation of ROIs is not significantly different from the arithmetic sum of single ROI responses at all tested holding potentials (spikes were removed by low-pass filtering at 13 Hz, n = 5 KCs, p = 0.50, two-way ANOVA with repeated measurements).

RESULTS

KCs Add Inputs from Multiple PNs Linearly

Anatomically, KCs receive inputs from seven PNs on average (Caron et al., 2013). In response to odors, KCs generate action potentials by integrating coincident inputs from multiple PNs (Gruntman and Turner, 2013). Therefore, it is important to determine how multiple subthreshold synaptic inputs interact in KCs. A previous study examined this issue by stimulating an optogenetic probe expressed in a few glomeruli with light, and comparing the postsynaptic responses of KCs receiving various numbers of PN inputs (Gruntman and Turner, 2013). However, combinations of only three, fixed glomeruli were tested and the comparison was made between KC responses in different animals. Therefore, it remains to be investigated how individual KCs integrate synaptic inputs from multiple PNs belonging to various glomeruli.

We tackled the problem by optogenetically activating diverse sets of PNs connected to single KCs either sequentially or simultaneously and comparing the postsynaptic responses. We achieved this with two-photon excitation of an optogenetic probe because it provides higher spatial resolution than optogenetic activation with a continuous wave laser (Andrasfalvy et al., 2010). Specifically, we expressed ReaChR (Inagaki et al., 2014; Lin et al., 2013) in PNs in 44 out of ~51 glomeruli and targeted a subset of them with a pulsed laser (Figures 1B, S1A, and S1B and Table S1). To stimulate individual glomeruli, we separately excited 6 × 6 regions of interest (ROIs, 12 μm × 12 μm each) placed every 5 μm along the depth to cover the entire antennal lobe (Figure 1C, see STAR Methods).

Two-photon excitation effectively depolarized PNs in all the ReaChR-positive glomeruli tested (25/25 glomeruli; Figure S1C). Excitation with stronger laser power made these responses exceed the spiking threshold (Figure S1D). The laser power was kept at an appropriate level to retain the high spatial resolution of optogenetic activation while evoking spikes in a substantial number of glomeruli (15/25 glomeruli; Figures 1D, S1E, and S1G). These spiking responses were reliable (Figure S1F). The

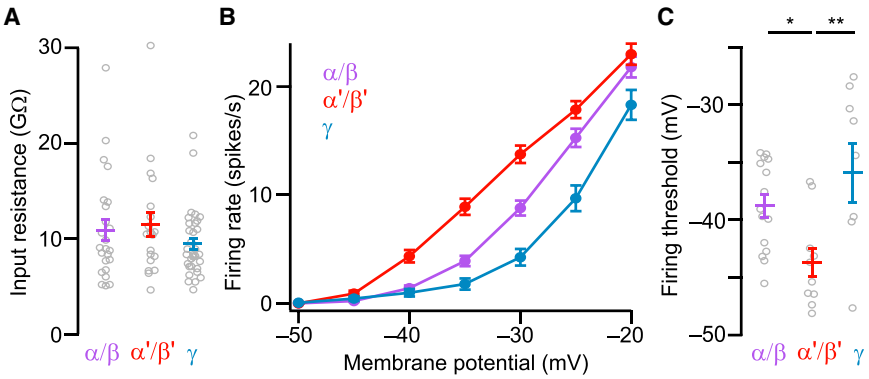

Figure 2. α′/β′ KCs Are Intrinsically the Most Excitable

(A) Input resistance measured at soma is not significantly different between cell types (n = 24, 19, 33 for α/β, α′/β′, and γ KCs, respectively; p = 0.30, one-way ANOVA).

(B) Relationship between the KC membrane potential and the firing rate. Membrane potential changes were elicited by injecting currents into the KC soma, and the mean firing rate was measured for each level of depolarization. The rank order of excitability is α′/β′ to α/β to γ. n = 15, 10, 7 for α/β, α′/β′, and γ KCs, respectively.

(C) α′/β′ KCs have the lowest firing threshold (n = 15, 10, 8 for α/β, α′/β′, and γ KCs, respectively; *p < 0.05, **p < 0.01, one-way ANOVA with post hoc Tukey HSD).

same stimulation also evoked clear postsynaptic responses in KCs (Figures 1D and S1G). PNs showed strong spiking responses in one ROI and weaker responses in neighboring, orthogonal ROIs (Figure S1H). The lateral resolution (full width at half maximum = 15.8 μm) was comparable to the typical diameter of a glomerulus (~10 to 15 μm, Figure S1I). As indicated by theoretical studies (Helmchen and Denk, 2005; Rickgauer and Tank, 2009), the axial resolution was relatively lower than the lateral resolution (full width at half maximum = 25.7 μm, Figure S1I). These results suggest that stimulation of a single ROI approximately corresponds to stimulation of a single glomerulus.

To examine how KCs integrate inputs from multiple PNs, we first activated two ROIs individually while recording from KCs (Figures 1E and 1F). We then stimulated these two ROIs nearly simultaneously (coactivation in Figure 1F) and compared the response to a simple summation of KC responses to individual stimulations (arithmetic sum in Figure 1F). The coactivated response matched the arithmetic sum. We tested various combinations of ROIs and found that responses were always combined linearly or slightly sublinearly in all KC types (Figure 1G). This relationship did not deviate much even for the integration of three ROIs (Figure 1H). These results demonstrate that, at the subthreshold level, KCs pool inputs from multiple PNs close to linearly, irrespective of the identity of glomeruli.

KCs do not show voltage-dependent boosting of synaptic inputs (Gruntman and Turner, 2013; Murthy et al., 2008). This argues that integration of inputs from two ROIs should not depend on the KC membrane potential. As expected, KCs combined dendritic inputs linearly at every holding membrane potential examined (Figure 1I). Smaller responses at higher holding potentials can be explained by a decrease in electrical driving force across the cellular membrane (Murthy et al., 2008).

α′/β′ KCs Are Intrinsically More Excitable

To understand how depolarizing input will lead to spikes in KCs, we examined the relationship between the membrane potential and the firing rate by injecting different amount of currents to the cell body. We found that, despite the similarity in input resistance measured at the soma (Figure 2A), the ability to generate spikes varied across cell types (Figure 2B). The rank order of excitability was α′/β′, α/β, and γ. α′/β′ KCs had a lower firing threshold compared to the other two cell types (Figure 2C). Intriguingly, this order of excitability can account for the previously reported rank order of broadness of odor tuning, spontaneous firing rate, and odor-evoked firing rate (Turner et al., 2008). These results suggest that the intrinsic property of KCs contributes to cell-type-specific olfactory processing in the MB (see below for further examination).

PN Activation Recruits Local, GABAergic Inhibition

We found that activation of PNs also recruits inhibition in KCs. To simultaneously activate a larger number of PNs than in the case of two-photon optogenetics experiments, we expressed ReaChR in 13 PNs using *Mz19-Gal4* and activated it with wide-field illumination (Gruntman and Turner, 2013; Jefferis et al., 2004). We confirmed that LED light can make *Mz19-Gal4*-positive PNs spike vigorously (Figure S3A). When these PNs were optogenetically stimulated with higher intensity of light, excitatory KC responses were followed by more salient, slow inhibition (Figures 3A and 3B). Different KCs exhibited different amount of inhibition (Figure S3B). This illustrates that individual KCs integrate both excitatory and inhibitory inputs.

It has been shown that strong input to the MB activates APL neuron, which provides feedback inhibition to KCs (Lin et al., 2014). This inhibition was described as all-to-all inhibition, because APL neuron inhibited all KCs at a time and blockade of output from all KCs was necessary to suppress the inhibition. Such a wide-spread inhibition, which we term here as global inhibition, is also observed in the locust MB (Papadopoulou et al., 2011).

To facilitate the characterization of inhibitory input to KCs, we isolated the lateral inhibitory component by recording from KCs that were not directly connected with boutons of *Mz19-Gal4*-positive PNs (Figure 3C, see STAR Methods). Clear inhibition was induced by light stimulation but, unexpectedly, not in all KCs (Figure 3D). Some KCs were almost not hyperpolarized at all, suggesting that the inhibition is effective locally (Figure 3E). The lack of hyperpolarization is unlikely to be related to the health of the cell because these KCs showed normal input resistance and spiked in response to current injection to the soma.

Even though a single APL neuron innervates the entire MB, we still hypothesized that it is the origin of this local inhibition from the following reasons. First, APL neuron is a putative analog of the locust giant GABAergic neuron (GGN), which has a single

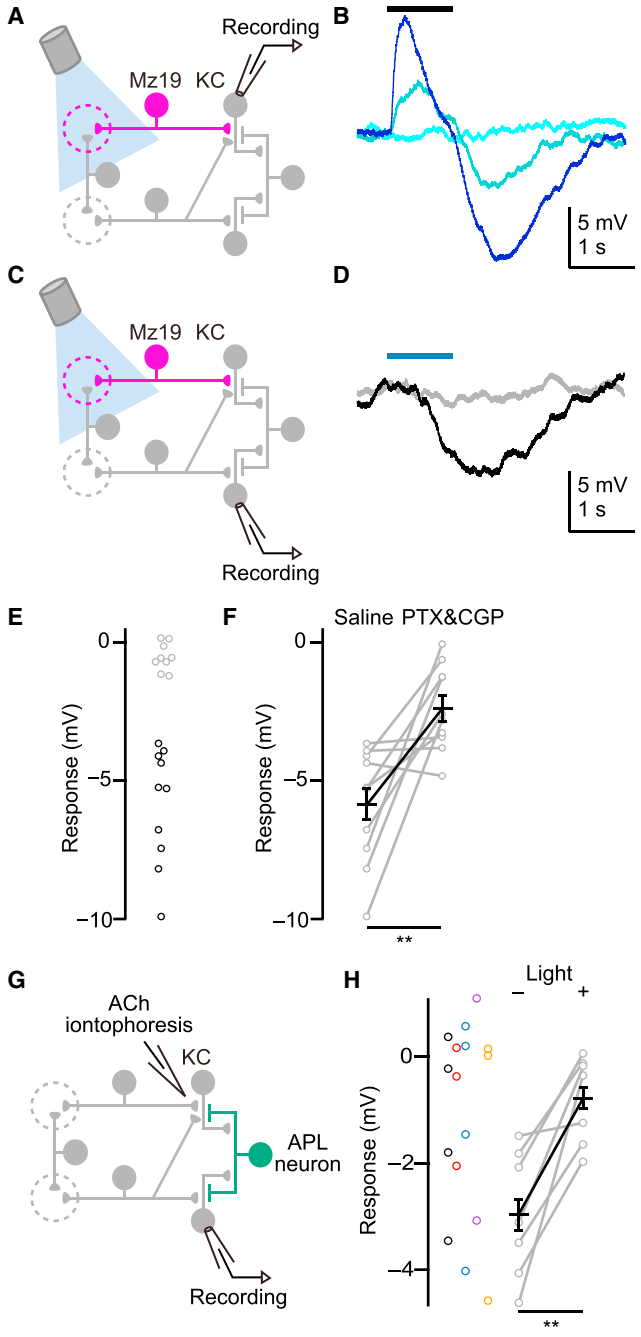

Figure 3. Input to the MB Recruits Local, Lateral Inhibition from APL Neurons

(A) Schematic of an experiment. *Mz19-Gal4*-positive PNs expressing ReaChR were stimulated with LED light. Recordings were made from KCs connected to *Mz19-Gal4*-positive PNs.

(B) Sample recording of KC responses to light at three different intensities (0.7, 1.9, and 11 μW). Stronger stimulation recruited stronger excitation and offset inhibition. Each trace is an average of three trials.

(C) Schematic of an experiment. *Mz19-Gal4*-positive PNs expressing ReaChR were stimulated with LED light. Recordings were made from KCs that were not connected with *Mz19-Gal4*-positive PNs.

(D) Responses of two KCs to light stimulation. Both are α′/β′ KCs. Light intensity is 6.5 μW. Blue bar, light stimulation. Each trace is an average of three trials.

(E) KCs were classified by unsupervised (k-means) clustering into two groups that did (black) or did not (gray) receive inhibition (n = 19 KCs). Offset responses were measured at 500 ms after the removal of light.

(F) Inhibitory offset responses were significantly suppressed by GABA receptor antagonists (**p < 0.01, paired t test, n = 10).

(G) Schematic of an experiment. KCs were activated by iontophoresis of acetylcholine (ACh) into the MB calyx. Archaerhodopsin (Arch) was expressed in APL neurons. To ensure that the recruited inhibition is local, at least two KCs were recorded from the same brain, and the current amplitude that evoked inhibition in a fraction of KCs was used for stimulation (Figure S3D).

(H) KC responses to iontophoresis. Data obtained from the same brain are plotted in the same color (n = 16 KCs from 5 brains). Offset responses were measured 300 ms after the removal of the current. Light activation of Arch significantly decreased the inhibitory offset response (**p < 0.01, paired t test, n = 7 KCs from 5 brains). Light was applied continuously throughout the response period.

cell body per hemisphere and provides inhibitory feedback to KCs (Papadopoulou et al., 2011). GGN is a non-spiking neuron. Non-spiking neurons rely on the graded potential but not action potentials to release neurotransmitters (Burrows and Siegler, 1976; Graubard, 1978). Therefore, APL neuron may utilize graded potential to release vesicles from a subset of neurites. Second, because APL neuron expresses presynaptic and postsynaptic markers throughout the neurite (Wu et al., 2013), the interactive loop between KCs and APL neuron can be closed locally at any part of the neurite.

To test this hypothesis, we first examined the neurotransmitter responsible for the inhibition. Consistent with the reports that APL neuron is immunopositive for GABA (Liu and Davis, 2009; Tanaka et al., 2008), antagonists for $GABA_A$ and $GABA_B$ receptors (picrotoxin [PTX] and CGP54626 [CGP], respectively) significantly decreased the inhibition (Figure 3F). Next, to directly examine whether APL neuron is the origin of local inhibition, we expressed an optogenetic silencer archaerhodopsin (Arch; Chow et al., 2010) with *APL-Gal4* (Figure S3C; Wu et al., 2013) and suppressed the activity of APL neuron. To induce inhibition, we mimicked the inputs from PNs to KCs by iontophoresing acetylcholine (ACh), a neurotransmitter released from PNs, into the MB calyx (Figure 3G). The strength of the input to the MB was controlled by adjusting the current for iontophoresis. With this approach, we were able to isolate a purely inhibitory component in some KCs. To ensure that the induced inhibition remains local, we confirmed that some other KCs in the same brain showed no response under the identical iontophoresis condition (Figure S3D). Under this setting, we found that light activation of Arch significantly decreased the inhibition (Figures 3H and S3E), indicating that the local inhibition originates from APL neuron.

α′/β′ KCs Preferentially Recruit Inhibition from APL Neuron

Previous studies suggest that KCs directly activate APL neuron (Lin et al., 2014; Yasuyama et al., 2002). To examine how KCs recruit inhibition from APL neuron, we evoked action potentials in single KCs by injecting a current to their cell body and measured the feedback inhibition (Figure 4A), an approach applied to characterize a dendrodendritic feedback loop between mitral/tufted cells and inhibitory granule cells in the rodent olfactory bulb (Chen et al., 2000; Isaacson and Strowbridge, 1998). We found

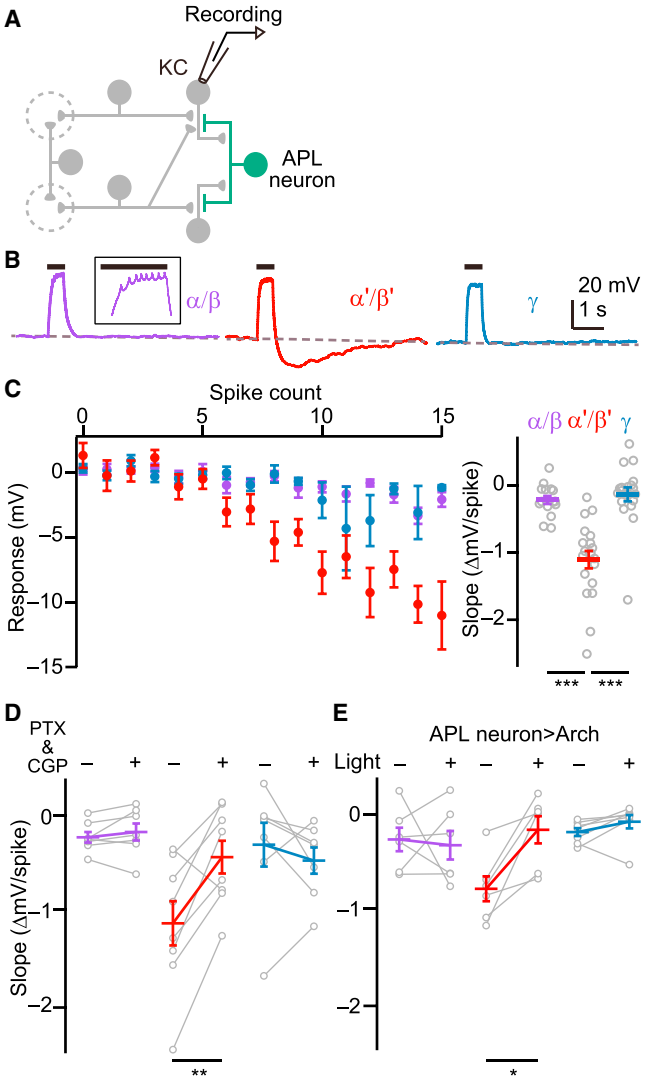

Figure 4. KC-Type-Specific Recruitment of GABAergic Inhibition via APL Neurons

(A) Schematic of an experiment.

(B) Typical KC traces showing a cell-type-specific inhibitory offset response following spikes. Spikes were evoked in KCs (inset) by injecting a current into the soma for 500 ms (black bar). α′/β′ KCs show a stronger inhibitory offset response compared to the other two cell types. Dotted line indicates the resting potential.

(C) Left: relationship between the KC spike count in 500 ms and the offset response measured 500 ms after the end of current injection (5–40 pA). Right: the slope of a line fit separately to data from each KC types within the linear range (3 to 15 spikes). The slope for α′/β′ KCs is significantly steeper than that for the other two cell types (***$p < 0.001$, one-way ANOVA with post hoc Tukey HSD; n = 15, 19, 19 for α/β, α′/β′, and γ KCs, respectively).

(D) The slope for α′/β′ KCs was significantly decreased by GABA receptor antagonists (**$p < 0.01$, paired t test with Bonferroni correction; n = 7, 8, 7 for α/β, α′/β′, and γ KCs, respectively).

(E) Light activation of Arch expressed in APL neurons significantly decreased the slope for α′/β′ KCs (*$p < 0.05$, paired t test with Bonferroni correction; n = 6, 6, 7 for α/β, α′/β′, and γ KCs, respectively).

that activation of single KCs recruits a hyperpolarizing offset response, but unexpectedly, only prominently in α′/β′ KCs (Figure 4B). Stronger activation of each KC proportionally induced larger offset responses in α′/β′ KCs, whereas responses remained small in the other two cell types (Figure 4C). KC spikes were necessary to evoke this offset response because it was abolished by the addition of tetrodotoxin (Figure S4). The offset response does not reflect intrinsically generated slow afterhyperpolarization as it was significantly reduced by GABA receptor antagonists (Figure 4D). Strong reduction in inhibition upon optical suppression of APL neuron further confirmed that the synaptic inhibition is mediated by APL neuron (Figure 4E). These results revealed that α′/β′ KCs preferentially recruit GABAergic feedback inhibition via APL neuron.

APL Neuron Can Inhibit All Types of KCs with a Similar Strength

This cell-type-specific inhibition can be explained by two mechanisms. One possibility is that α′/β′ KCs activate APL neuron more strongly than the other two types so that, in turn, they receive stronger inhibition. Another possibility is that although all three types of KCs can activate APL neuron equally, α′/β′ KCs are more sensitive to inhibitory input from APL neuron. To evaluate these possibilities, we optogenetically activated APL neurons using CsChrimson (Klapoetke et al., 2014) and recorded responses from every type of KC (Figure 5A). We found that responses were mediated by both $GABA_A$ and $GABA_B$ receptors (Figures 5B and 5C) and, critically, similar in strength between all types of KCs (Figures 5D and 5E). This result suggests that cell-type specificity of inhibition originates in the ability of α′/β′ KCs to activate APL neuron more strongly than the other two cell types. Furthermore, inhibition was observed in every single KC we examined, implying that APL neuron can modulate all ~2,000 KCs.

The Spatial Extent of APL Neuron Activity Can Be Lobe Specific or Global Depending on the Olfactory Input to the MB

If α′/β′ KCs had the privilege of preferentially recruiting APL neurons on top of higher intrinsic excitability (Figure 2), branches of APL neuron in the α′/β′ lobe should be activated first as olfactory input to the MB is gradually increased. To test this, we expressed the genetically encoded Ca^{2+} indicator GCaMP6s (Chen et al., 2013) in APL neurons and used two-photon microscopy to visualize their response to a strong odor (ethyl butyrate) diluted over a wide range (Figure 6A). We imaged GCaMP signals in three medial lobes (β, β′, and γ; Figures 6B and 6C). As expected, we consistently observed Ca^{2+} responses in the β′ lobe even to low concentrations of odor (10^{-9} and 10^{-7}), which only evoked negligible responses in the other two lobes (Figures 6D and 6E). When we gradually increased the concentration, signals appeared and grew in β and γ lobes as well (Figure 6E). This is in line with our earlier observation that optogenetic activation of APL neuron can inhibit all KCs of all types (Figure 5). Together, these results demonstrate that neurites of APL neuron in the β′ lobe are indeed preferentially activated and APL neuron responds in a lobe-specific to global manner flexibly depending on the strength of the olfactory stimulus.

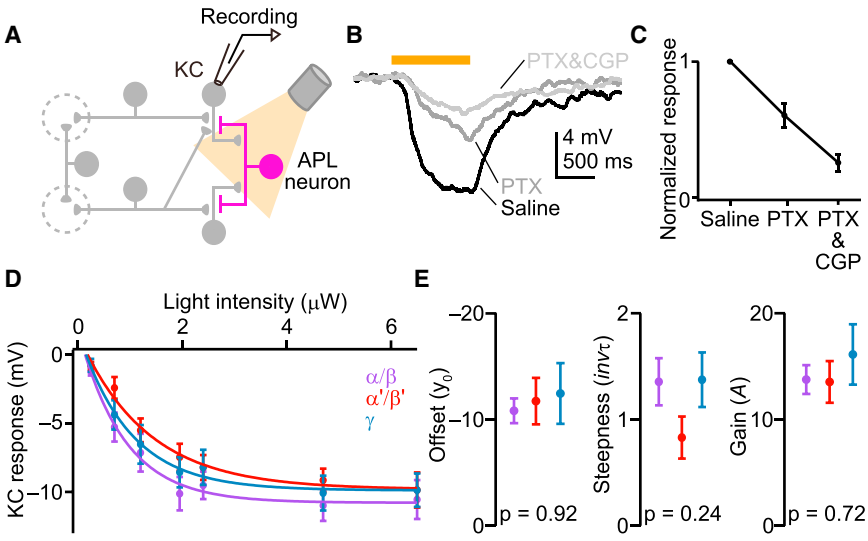

Figure 5. Optogenetic Activation of APL Neurons Inhibit All Types of KCs with a Similar Strength

(A) Schematic of an experiment. CsChrimson expressed in APL neurons was activated with amber LED light.

(B) KC responses to optogenetic activation of APL neurons with or without the presence of GABA receptor antagonists. Each trace is an average of three trials.

(C) KCs receive inhibition from APL neurons through both $GABA_A$ and $GABA_B$ receptors (n = 10 KCs).

(D) Optogenetic activation of APL neurons at various light intensities (n = 5, 8, 9 for α/β, α′/β′, and γ KCs, respectively). The smooth lines are fit to the data with an exponential function: $f(\text{Light intensity}) = y_0 + A\exp\{-inv\tau \cdot (\text{Light intensity})\}$

(E) Three parameters that determine the shape of the exponential fit in (D) are not significantly different between cell types. p values are shown in each panel (one-way ANOVA).

α′/β′ KCs Are More Responsive and Sensitive to Odor Presentation and Carry More Information about Odor Concentrations than Other KC Types

Given these differential physiological properties of KC types, one can infer that several aspects of KC responses to odors should also be cell-type specific. First, because α′/β′ KCs are intrinsically more excitable, these neurons are expected to detect odors more rapidly. To test this hypothesis, we expressed GCaMP5 (Akerboom et al., 2012) in all KCs under the control of *OK107-Gal4* (Connolly et al., 1996) and imaged the medial lobes (Figure 7A). We found that α′/β′ KCs, indeed, responded to ethyl butyrate with shorter latency as compared to the other two cell types (Figures 7B–7D). Therefore, having α′/β′ KCs in the circuit is beneficial in speeding up the detection of odors.

Second, from the same reason, α′/β′ KCs are likely to be more sensitive to olfactory stimuli. As expected, α′/β′ KCs showed significantly larger responses to ethyl butyrate at low concentrations (10^{-9} and 10^{-7}) than the other two cell types, which remained nearly unresponsive to these stimuli (Figure 8A). Responses of α′/β′ KCs increased gradually with concentration and remained strongest among responses of three cell types at all concentrations examined (Figure 8A).

This result further suggests that α′/β′ KCs can better discriminate between different, especially low concentrations of odors. To test this, we quantified whether responses of α′/β′ KCs carry more information about the identity of the concentration using linear discriminant decoding analysis. To quantify the decoding accuracy, for each cell type, we withheld one response from the entire data (responses to four repeated presentations of odors at five different concentrations), trained the decoder with the remaining data, and predicted the identity of the concentration that evoked the withheld response (see STAR Methods). As hypothesized, decoding accuracy was higher for α′/β′ KCs at low concentrations (10^{-9} or 10^{-7}), while performance was comparable across three cell types at higher concentrations ($\geq 10^{-5}$) (Figure 8B).

Because the balance between excitation and inhibition is important for the stability of a system, we finally asked whether this high discriminability of α′/β′ KCs may be compromised by suppressing the feedback inhibition, which should normally control both the overall gain and the trial-to-trial fluctuation of excitatory input. Given that α′/β′ KCs receive the strongest GABAergic inhibition from APL neurons (Figure 4) and branches of APL neurons are most strongly activated by odors in the β′ lobe (Figure 6), we further hypothesized that blockade of GABAergic transmission in all three KCs will have the largest effect on α′/β′ KCs. Indeed, although application of GABA receptor antagonists made the responses larger and more variable in all cell types, disinhibition of mean response to low concentrations of odor was particularly prominent in α′/β′ KCs (Figure 8C). Consequently, the dynamic range calculated as a difference between normalized responses to the highest and lowest concentration of odor became significantly narrower in α′/β′ KCs (Figure 8D). To examine how this decrease in the dynamic range and increase in variability together affect the discriminability between olfactory stimuli, we again performed a decoding analysis and found that the discriminability became lower in the presence of GABA receptor antagonists in α′/β′ KCs (Figure 8E). These results suggest that feedback inhibition matched with the higher excitability is crucial for α′/β′ KCs to discriminate between olfactory stimuli of various strengths.

DISCUSSION

Linear Mixing of Excitatory Inputs in KCs

In an attempt to understand how multiple PN inputs are integrated in KCs, a previous study reported that responses of KCs are correlated with the number of PN inputs (Gruntman and Turner, 2013). However, synaptic integration remained to be investigated because the comparison was made between KCs in different animals and not within the same cell. Another study in rodents instead showed that coactivation of olfactory

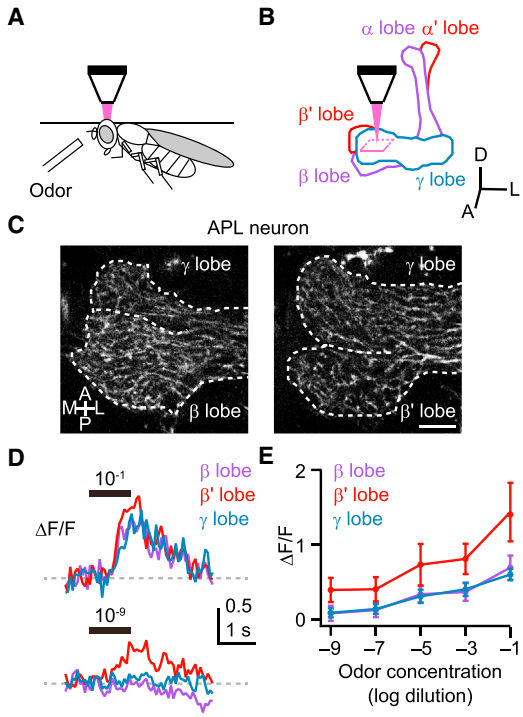

Figure 6. The Spatial Extent of Calcium Responses in APL Neuron Shifts from Lobe-Specific to Global with Increasing Olfactory Input to the MB

(A) Schematic of an experiment. Odor responses of APL neurons were recorded with calcium imaging. GCaMP6s was expressed in APL neurons with *VT43924-Gal4*.

(B) GCaMP signals were recorded from three medial lobes. A, anterior, D, dorsal, L, lateral.

(C) Baseline signal of GCaMP6s. The dotted lines indicate the boundaries of different medial lobes. Odor responses were recorded at the tip of the lobes where different lobes can be clearly segregated. Dorsal view. Scale bar, 10 μm. A, anterior, P, posterior, L, lateral, M, medial.

(D) Sample recording (mean ΔF/F in 16.64 μm × 16.64 μm ROI averaged across four trials) from three lobes in response to ethyl butyrate at 10^{-1} (top) or 10^{-9} (bottom) dilution. Black bar, odor application (1 s).

(E) Responses of APL neuron in three lobes to ethyl butyrate at various concentrations. Neurites in the β′ lobe showed substantially larger responses as compared to those in the other two lobes ($p < 0.001$, two-way ANOVA with repeated measurements; β versus β′ and β′ versus γ, $p < 0.001$, post hoc Tukey HSD; n = 6 flies).

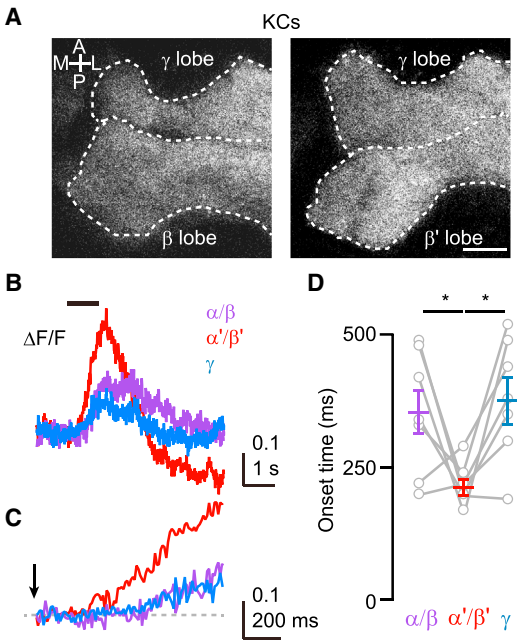

Figure 7. α′/β′ KCs Respond to Odors with Shorter Latency

(A) Baseline signal of GCaMP5 expressed in all KCs with *OK107-Gal4*. The dotted lines indicate the boundaries of different medial lobes. Signals were imaged and analyzed as in Figure 6. Dorsal view. Scale bar, 10 μm. A, anterior, P, posterior, L, lateral, M, medial.

(B) Sample recording from three types of KCs in response to ethyl butyrate (10^{-1} dilution). Black bar, odor application (1 s). Each trace is an average of ten trials.

(C) Enlarged view of calcium responses during odor application period shown in (B). Arrow indicates the onset of the odor.

(D) Onset time of GCaMP signals. α′/β′ KCs start to respond earlier than the other two cell types (*$p < 0.05$, one-way ANOVA with post hoc Tukey HSD; n = 7 flies).

bulb glomeruli with glutamate uncaging induced supralinear postsynaptic responses in the piriform cortex (Davison and Ehlers, 2011). Here, we activated individual glomeruli with precision using two-photon optogenetics and found that KCs sum inputs from multiple PNs linearly, irrespective of the identity of glomeruli. Because we have likely sampled PNs connected to KC claws, dendritic structures that enwrap PN boutons (Caron et al., 2013; Gruntman and Turner, 2013), at diverse physical locations, this indicates that KCs pool inputs equally from any combination of claws. Importantly, each KC receives on average seven inputs from a random set of PNs (Caron et al., 2013) with some local rules (Gruntman and Turner, 2013). Therefore, our results suggest that ~2,000 KCs mix different aspects of olfactory information reaching their claws equally to create diverse odor representations. This functional organization of the MB circuit is advantageous in that it represents odors distinctively in a high-dimensional coding space and thus can enhance odor discriminability (Babadi and Sompolinsky, 2014; Litwin-Kumar et al., 2017).

Local and Global Modes of Inhibition by Single APL Neurons

As PNs were more strongly activated, KCs not only showed enhanced excitation but also inhibition. Inhibition followed excitation by several hundred ms and were often strong enough to override the initial depolarization (Figures 3B and S3B). This is likely one mechanism that generates spatially (Honegger et al., 2011; Lin et al., 2014) and temporally sparse odor representations in KCs (Murthy et al., 2008; Turner et al., 2008). In the locust KCs (Perez-Orive et al., 2002) and the rodent piriform cortex neurons where odors are encoded sparsely (Poo and Isaacson, 2009), excitatory input is similarly followed by global inhibition found in most cells.

What was different from the previous studies was that the effect of inhibition can be local: some KCs received prominent

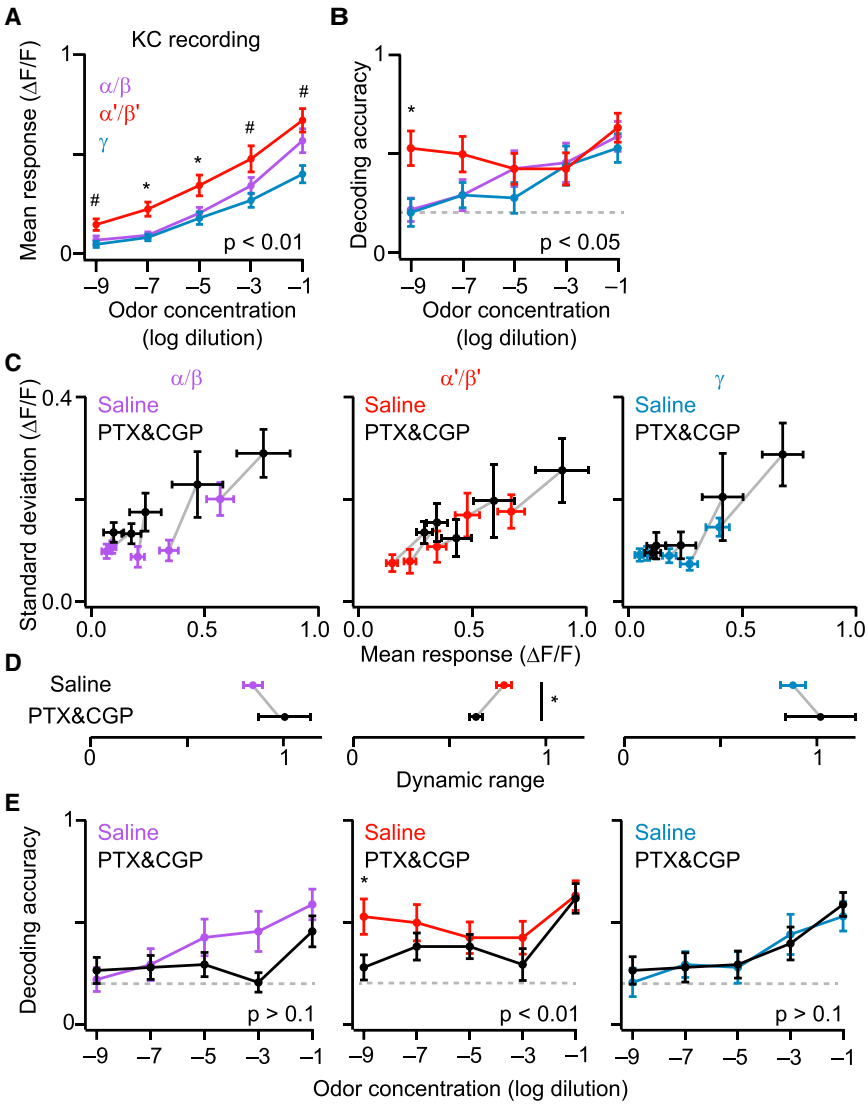

Figure 8. Higher Sensitivity of α′/β′ KCs and Cell-Type-Specific Inhibition Enhances Discrimination between Different Odor Concentrations

(A) Activity of KCs recorded in medial lobes in response to various concentrations of ethyl butyrate. The same genotype as in Figure 7. α′/β′ KCs respond more strongly than the other two cell types. p value of two-way ANOVA with repeated measurements (difference between cell types) is shown in the panel. Asterisks (*) denote significant differences ($p < 0.05$, Tukey HSD) for α/β versus α′/β′ and for α′/β′ versus γ, hashes (#) denote significant differences for α′/β′ versus γ. n = 17 flies (same flies across all the panels in Figure 8).

(B) Accuracy of decoding odor concentrations using linear discriminant analysis. The dotted line indicates chance performance. Accuracy was significantly different between cell types. p value (difference between cell types) is shown in the panel (two-way ANOVA with repeated measurements; *$p < 0.05$, α′/β′ versus γ, Tukey HSD).

(C) Application of GABA receptor antagonists increases both response amplitude (mean ΔF/F) and trial-to-trial variability (standard deviation) in all cell types (mean and standard deviation were calculated from responses to the same stimuli in four trials; $p < 0.05$, two-way ANOVA with repeated measurements, saline versus PTX and CGP). Gray line connects responses to the same concentration of odor.

(D) GABA receptor antagonists narrow the dynamic range, defined as the difference in normalized responses to 10^{-1} and 10^{-9} dilutions (see STAR Methods) in α′/β′ KCs (*$p < 0.05$, paired t test with Bonferroni correction).

(E) Application of GABA receptor antagonists decreases the performance of decoding in α′/β′ KCs. p values are shown in each panel (two-way ANOVA with repeated measurements, saline versus PTX and CGP. *$p < 0.05$, Tukey HSD). The dotted line indicates chance performance.

inhibition while others in the same brain received none (Figures 3 and S3D). Moreover, activation of single KCs by current injection was sufficient to induce feedback synaptic inhibition (Figure 4). Our optogenetic silencing experiment demonstrated that this was mediated by GABAergic APL neurons even though they have been reported to innervate throughout the MB and only mediate global inhibition (Lin et al., 2014). Therefore, APL neurons can exert inhibition both locally and globally. Because APL neuron is excited by KCs (Lin et al., 2014), this local processing represents an efficient solution to provide inhibition matched with the level of KC activity without necessarily inhibiting the whole system. This suggests that APL neuron serves a role in addition to the global gain control that maintains the sparseness of odor representations in the MB (Lin et al., 2014).

How, then, does a single neuron innervating the entire MB inhibit KCs locally? Two factors suggest dendrodendritic (or neurite-to-neurite) release as a mechanism for local inhibition. First, ectopically expressed pre- and postsynaptic markers in APL neurons distribute throughout the MB (Wu et al., 2013), implying that the recurrent loop between KCs and APL neuron may close within a local region. Second, the locust analog of APL neuron is non-spiking (Papadopoulou et al., 2011), making graded release of neurotransmitter likely in APL neuron as well. In fact, at least APL neuron does not seem to spike within an input range that evokes localized GCaMP signals in only one of the lobes (Figure 6). If spikes had been generated, we should have observed global signals in APL neuron because spikes generally elevate calcium concentration throughout the cell (Smetters et al., 1999; Yuste and Denk, 1995). This mechanism is reminiscent of that in the mammalian olfactory bulb in which granule cells mediate lateral inhibition through dendrodendritic release in response to inputs from mitral/tufted cells (Chen et al., 2000; Isaacson and Strowbridge, 1998).

There exists another set of GABAergic neurons in the MB, dorsal paired medial (DPM) neurons, that are qualified to mediate this inhibition. In each hemisphere, DPM neuron innervates the

entire MB except for the calyx (Tanaka et al., 2008) and connects with APL neuron via gap junctions (Wu et al., 2011). Therefore, there is a possibility that DPM neurons are also involved in inhibiting KCs.

Cell-Type-Specific Mechanisms Enhance Odor Detection Speed and Discrimination between Different Odor Concentrations in α′/β′ KCs

Three types of KCs pooled PN inputs in a similar manner (Figures 1 and S2). However, upon depolarization, α′/β′ KCs spiked most readily, followed in order by α/β and γ KCs (Figure 2). This mirrors the rank order of broadness of odor tuning, spontaneous firing rate, and odor-evoked firing rate (Turner et al., 2008), suggesting that the intrinsic mechanism of spike generation is one of the origins of cell-type-specific responses in KCs. The heterogeneity in intrinsic excitability may reflect differential possession of voltage-sensitive conductances as recent transcriptome analyses revealed that the gene expression profile is different between KC types (Crocker et al., 2016; Perrat et al., 2013).

Incidentally, α′/β′ KCs were also the most effective in recruiting feedback inhibition by APL neurons (Figure 4). This can be either due to preferential activation of APL neuron by α′/β′ KCs or preferential inhibition of α′/β′ KCs by APL neuron. Our results supported the former because optogenetic activation of APL neurons inhibited all three types of KCs equally (Figure 5). This conclusion was corroborated by our additional observation that APL neuron exhibits highest sensitivity and responsiveness to odors in the β′ lobe (Figure 6). How do α′/β′ KCs more effectively activate APL neuron? First factor is their higher intrinsic excitability. Because they generate spikes more readily, the total drive to the APL neuron will be larger under a particular input to the MB. Second is their stronger functional connection with the APL neuron. Because the same number of spikes evoked larger inhibition in α′/β′ KCs (Figure 4C), these cells likely form stronger or more abundant synapses with APL neurons. This is in line with the anatomical observation that APL neurons contact most densely with α′/β′ KCs in the lobes (Pitman et al., 2011).

The three types of KCs have been morphologically subdivided into finer categories in some studies (Aso et al., 2014a; Costa et al., 2016; Lin et al., 2007; Tanaka et al., 2008). In terms of function, α/β core and α/β surface KCs, for example, are shown to be involved in different aspects of olfactory learning (Perisse et al., 2013). Therefore, although we did not find clear clusters in our data within each of the three conventional cell types, there may be additional complexity in cell-type specificity.

Based on the differences in physiological properties between KC types, we were able to predict and confirm previously unidentified functions of α′/β′ KCs in odor processing. As suggested by higher intrinsic excitability, α′/β′ KCs detected ethyl butyrate with shortest latency and highest sensitivity (Figures 7 and 8). This allowed α′/β′ KCs to discriminate between different odor concentrations most accurately, which required balanced feedback inhibition by APL neuron (Figure 8). These results indicate that, by having α′/β′ KCs, the MB circuit can enhance the detection speed, sensitivity, and discriminability of different odor concentrations. Notably, the actual decoders of the KC activity, the MB output neurons, innervate particular compartments in the lobes to contact generally one of three KC types (Aso et al., 2014a). These MB output neurons encode valence and bias the behavior toward attraction or aversion in various learning tasks (Aso et al., 2014b; Owald et al., 2015). Therefore, the MB output neurons innervating the α′/β′ lobes may shape the fly's initial behavioral response to an odor and that with a higher sensitivity and discriminability.

STAR★METHODS

Detailed methods are provided in the online version of this paper and include the following:

- KEY RESOURCES TABLE
- CONTACT FOR REAGENT AND RESOURCE SHARING
- EXPERIMENTAL MODEL AND SUBJECT DETAILS
  - Flies
- METHOD DETAILS
  - Electrophysiology
  - Immunohistochemistry
  - Iontophoresis
  - Stimulation of optogenetic probes
  - Calcium imaging
- QUANTIFICATION AND STATISTICAL ANALYSIS

SUPPLEMENTAL INFORMATION

Supplemental Information includes four figures and two tables and can be found with this article online at http://dx.doi.org/10.1016/j.neuron.2017.06.039.

AUTHOR CONTRIBUTIONS

K.I. performed the experiments and analyzed the data. Y.T. generated the new transgenic fly line. K.I. and H.K. designed the experiments and wrote the paper.

ACKNOWLEDGMENTS

We thank Ann-Shyn Chiang, Barry Dickson, Kei Ito, Adrian Moore, Vivek Jayaraman, Vienna Drosophila Resource Center, Bloomington Stock Center, and Developmental Studies Hybridoma Bank for fly stocks and reagents; Edward Boyden for the FCK-Arch-GFP plasmid; and RIKEN BSI-Olympus Collaboration Center for the microscopy services. We are grateful to Yoshinori Aso, Toshihide Hige, and Akinao Nose for their comments on the earlier version of the manuscript; Kazuo Okanoya for his guidance; and members of the Kazama laboratory for their support and comments on the manuscript. K.I. was supported by the RIKEN JRA fellowship and a Grant-in-Aid for JSPS Research Fellow (13J00456). This work was funded by a grant from RIKEN, a grant from Kao Corporation, and Grants-in-Aid for Scientific Research (23680044, 25115732) from MEXT to H.K.

Received: January 10, 2017
Revised: May 23, 2017
Accepted: June 23, 2017
Published: July 19, 2017

REFERENCES

Akerboom, J., Chen, T.W., Wardill, T.J., Tian, L., Marvin, J.S., Mutlu, S., Calderón, N.C., Esposti, F., Borghuis, B.G., Sun, X.R., et al. (2012). Optimization of a GCaMP calcium indicator for neural activity imaging. J. Neurosci. *32*, 13819–13840.

Andrasfalvy, B.K., Zemelman, B.V., Tang, J., and Vaziri, A. (2010). Two-photon single-cell optogenetic control of neuronal activity by sculpted light. Proc. Natl. Acad. Sci. USA *107*, 11981–11986.

Ascoli, G.A., Alonso-Nanclares, L., Anderson, S.A., Barrionuevo, G., Benavides-Piccione, R., Burkhalter, A., Buzsáki, G., Cauli, B., Defelipe, J., Fairén, A., et al.; Petilla Interneuron Nomenclature Group (2008). Petilla terminology: nomenclature of features of GABAergic interneurons of the cerebral cortex. Nat. Rev. Neurosci. *9*, 557–568.

Aso, Y., Grübel, K., Busch, S., Friedrich, A.B., Siwanowicz, I., and Tanimoto, H. (2009). The mushroom body of adult *Drosophila* characterized by GAL4 drivers. J. Neurogenet. *23*, 156–172.

Aso, Y., Hattori, D., Yu, Y., Johnston, R.M., Iyer, N.A., Ngo, T.T., Dionne, H., Abbott, L.F., Axel, R., Tanimoto, H., and Rubin, G.M. (2014a). The neuronal architecture of the mushroom body provides a logic for associative learning. eLife *3*, e04577.

Aso, Y., Sitaraman, D., Ichinose, T., Kaun, K.R., Vogt, K., Belliart-Guérin, G., Plaçais, P.Y., Robie, A.A., Yamagata, N., Schnaitmann, C., et al. (2014b). Mushroom body output neurons encode valence and guide memory-based action selection in *Drosophila*. eLife *3*, e04580.

Babadi, B., and Sompolinsky, H. (2014). Sparseness and expansion in sensory representations. Neuron *83*, 1213–1226.

Badel, L., Ohta, K., Tsuchimoto, Y., and Kazama, H. (2016). Decoding of context-dependent olfactory behavior in *Drosophila*. Neuron *91*, 155–167.

Bhandawat, V., Olsen, S.R., Gouwens, N.W., Schlief, M.L., and Wilson, R.I. (2007). Sensory processing in the *Drosophila* antennal lobe increases reliability and separability of ensemble odor representations. Nat. Neurosci. *10*, 1474–1482.

Bischof, J., Maeda, R.K., Hediger, M., Karch, F., and Basler, K. (2007). An optimized transgenesis system for Drosophila using germ-line-specific phiC31 integrases. Proc. Natl. Acad. Sci. USA *104*, 3312–3317.

Blum, A.L., Li, W., Cressy, M., and Dubnau, J. (2009). Short- and long-term memory in *Drosophila* require cAMP signaling in distinct neuron types. Curr. Biol. *19*, 1341–1350.

Burrows, M., and Siegler, M.V. (1976). Transmission without spikes between locust interneurones and motoneurones. Nature *262*, 222–224.

Caron, S.J., Ruta, V., Abbott, L.F., and Axel, R. (2013). Random convergence of olfactory inputs in the *Drosophila* mushroom body. Nature *497*, 113–117.

Cervantes-Sandoval, I., Martin-Peña, A., Berry, J.A., and Davis, R.L. (2013). System-like consolidation of olfactory memories in *Drosophila*. J. Neurosci. *33*, 9846–9854.

Chen, W.R., Xiong, W., and Shepherd, G.M. (2000). Analysis of relations between NMDA receptors and GABA release at olfactory bulb reciprocal synapses. Neuron *25*, 625–633.

Chen, T.W., Wardill, T.J., Sun, Y., Pulver, S.R., Renninger, S.L., Baohan, A., Schreiter, E.R., Kerr, R.A., Orger, M.B., Jayaraman, V., et al. (2013). Ultrasensitive fluorescent proteins for imaging neuronal activity. Nature *499*, 295–300.

Chow, B.Y., Han, X., Dobry, A.S., Qian, X., Chuong, A.S., Li, M., Henninger, M.A., Belfort, G.M., Lin, Y., Monahan, P.E., and Boyden, E.S. (2010). High-performance genetically targetable optical neural silencing by light-driven proton pumps. Nature *463*, 98–102.

Connolly, J.B., Roberts, I.J., Armstrong, J.D., Kaiser, K., Forte, M., Tully, T., and O'Kane, C.J. (1996). Associative learning disrupted by impaired Gs signaling in *Drosophila* mushroom bodies. Science *274*, 2104–2107.

Costa, M., Manton, J.D., Ostrovsky, A.D., Prohaska, S., and Jefferis, G.S. (2016). NBLAST: Rapid, sensitive comparison of neuronal structure and construction of neuron family databases. Neuron *91*, 293–311.

Crittenden, J.R., Skoulakis, E.M., Han, K.A., Kalderon, D., and Davis, R.L. (1998). Tripartite mushroom body architecture revealed by antigenic markers. Learn. Mem. *5*, 38–51.

Crocker, A., Guan, X.J., Murphy, C.T., and Murthy, M. (2016). Cell-type-specific transcriptome analysis in the *Drosophila* mushroom body reveals memory-related changes in gene expression. Cell Rep. *15*, 1580–1596.

Davison, I.G., and Ehlers, M.D. (2011). Neural circuit mechanisms for pattern detection and feature combination in olfactory cortex. Neuron *70*, 82–94.

Goodman, M.B., and Lockery, S.R. (2000). Pressure polishing: a method for re-shaping patch pipettes during fire polishing. J. Neurosci. Methods *100*, 13–15.

Graubard, K. (1978). Synaptic transmission without action potentials: input-output properties of a nonspiking presynaptic neuron. J. Neurophysiol. *41*, 1014–1025.

Gruntman, E., and Turner, G.C. (2013). Integration of the olfactory code across dendritic claws of single mushroom body neurons. Nat. Neurosci. *16*, 1821–1829.

Heisenberg, M. (2003). Mushroom body memoir: from maps to models. Nat. Rev. Neurosci. *4*, 266–275.

Helmchen, F., and Denk, W. (2005). Deep tissue two-photon microscopy. Nat. Methods *2*, 932–940.

Honegger, K.S., Campbell, R.A., and Turner, G.C. (2011). Cellular-resolution population imaging reveals robust sparse coding in the *Drosophila* mushroom body. J. Neurosci. *31*, 11772–11785.

Inagaki, H.K., Jung, Y., Hoopfer, E.D., Wong, A.M., Mishra, N., Lin, J.Y., Tsien, R.Y., and Anderson, D.J. (2014). Optogenetic control of *Drosophila* using a red-shifted channelrhodopsin reveals experience-dependent influences on courtship. Nat. Methods *11*, 325–332.

Isaacson, J.S., and Strowbridge, B.W. (1998). Olfactory reciprocal synapses: dendritic signaling in the CNS. Neuron *20*, 749–761.

Ito, K., Suzuki, K., Estes, P., Ramaswami, M., Yamamoto, D., and Strausfeld, N.J. (1998). The organization of extrinsic neurons and their implications in the functional roles of the mushroom bodies in *Drosophila melanogaster* Meigen. Learn. Mem. *5*, 52–77.

Jefferis, G.S., Vyas, R.M., Berdnik, D., Ramaekers, A., Stocker, R.F., Tanaka, N.K., Ito, K., and Luo, L. (2004). Developmental origin of wiring specificity in the olfactory system of *Drosophila*. Development *131*, 117–130.

Johnson, B.E., Brown, A.L., and Goodman, M.B. (2008). Pressure-polishing pipettes for improved patch-clamp recording. J. Vis. Exp. *20*, 964.

Kazama, H., and Wilson, R.I. (2009). Origins of correlated activity in an olfactory circuit. Nat. Neurosci. *12*, 1136–1144.

Klapoetke, N.C., Murata, Y., Kim, S.S., Pulver, S.R., Birdsey-Benson, A., Cho, Y.K., Morimoto, T.K., Chuong, A.S., Carpenter, E.J., Tian, Z., et al. (2014). Independent optical excitation of distinct neural populations. Nat. Methods *11*, 338–346.

Krashes, M.J., and Waddell, S. (2008). Rapid consolidation to a radish and protein synthesis-dependent long-term memory after single-session appetitive olfactory conditioning in *Drosophila*. J. Neurosci. *28*, 3103–3113.

Krashes, M.J., Keene, A.C., Leung, B., Armstrong, J.D., and Waddell, S. (2007). Sequential use of mushroom body neuron subsets during *drosophila* odor memory processing. Neuron *53*, 103–115.

Kudoh, S.N., and Taguchi, T. (2002). A simple exploratory algorithm for the accurate and fast detection of spontaneous synaptic events. Biosens. Bioelectron. *17*, 773–782.

Lee, T., and Luo, L. (1999). Mosaic analysis with a repressible cell marker for studies of gene function in neuronal morphogenesis. Neuron *22*, 451–461.

Lee, T., Lee, A., and Luo, L. (1999). Development of the *Drosophila* mushroom bodies: sequential generation of three distinct types of neurons from a neuroblast. Development *126*, 4065–4076.

Lin, H.H., Lai, J.S., Chin, A.L., Chen, Y.C., and Chiang, A.S. (2007). A map of olfactory representation in the *Drosophila* mushroom body. Cell *128*, 1205–1217.

Lin, J.Y., Knutsen, P.M., Muller, A., Kleinfeld, D., and Tsien, R.Y. (2013). ReaChR: a red-shifted variant of channelrhodopsin enables deep transcranial optogenetic excitation. Nat. Neurosci. *16*, 1499–1508.

Lin, A.C., Bygrave, A.M., de Calignon, A., Lee, T., and Miesenböck, G. (2014). Sparse, decorrelated odor coding in the mushroom body enhances learned odor discrimination. Nat. Neurosci. *17*, 559–568.

Litwin-Kumar, A., Harris, K.D., Axel, R., Sompolinsky, H., and Abbott, L.F. (2017). Optimal degrees of synaptic connectivity. Neuron *93*, 1153–1164.e7.

Liu, X., and Davis, R.L. (2009). The GABAergic anterior paired lateral neuron suppresses and is suppressed by olfactory learning. Nat. Neurosci. *12*, 53–59.

Markram, H., Muller, E., Ramaswamy, S., Reimann, M.W., Abdellah, M., Sanchez, C.A., Ailamaki, A., Alonso-Nanclares, L., Antille, N., Arsever, S., et al. (2015). Reconstruction and simulation of neocortical microcircuitry. Cell *163*, 456–492.

Murthy, M., Fiete, I., and Laurent, G. (2008). Testing odor response stereotypy in the *Drosophila* mushroom body. Neuron *59*, 1009–1023.

Owald, D., Felsenberg, J., Talbot, C.B., Das, G., Perisse, E., Huetteroth, W., and Waddell, S. (2015). Activity of defined mushroom body output neurons underlies learned olfactory behavior in *Drosophila*. Neuron *86*, 417–427.

Papadopoulou, M., Cassenaer, S., Nowotny, T., and Laurent, G. (2011). Normalization for sparse encoding of odors by a wide-field interneuron. Science *332*, 721–725.

Perez-Orive, J., Mazor, O., Turner, G.C., Cassenaer, S., Wilson, R.I., and Laurent, G. (2002). Oscillations and sparsening of odor representations in the mushroom body. Science *297*, 359–365.

Perisse, E., Yin, Y., Lin, A.C., Lin, S., Huetteroth, W., and Waddell, S. (2013). Different kenyon cell populations drive learned approach and avoidance in *Drosophila*. Neuron *79*, 945–956.

Perrat, P.N., DasGupta, S., Wang, J., Theurkauf, W., Weng, Z., Rosbash, M., and Waddell, S. (2013). Transposition-driven genomic heterogeneity in the *Drosophila* brain. Science *340*, 91–95.

Pfeiffer, B.D., Ngo, T.T., Hibbard, K.L., Murphy, C., Jenett, A., Truman, J.W., and Rubin, G.M. (2010). Refinement of tools for targeted gene expression in *Drosophila*. Genetics *186*, 735–755.

Pitman, J.L., Huetteroth, W., Burke, C.J., Krashes, M.J., Lai, S.L., Lee, T., and Waddell, S. (2011). A pair of inhibitory neurons are required to sustain labile memory in the *Drosophila* mushroom body. Curr. Biol. *21*, 855–861.

Poo, C., and Isaacson, J.S. (2009). Odor representations in olfactory cortex: "sparse" coding, global inhibition, and oscillations. Neuron *62*, 850–861.

Rickgauer, J.P., and Tank, D.W. (2009). Two-photon excitation of channelrhodopsin-2 at saturation. Proc. Natl. Acad. Sci. USA *106*, 15025–15030.

Smetters, D., Majewska, A., and Yuste, R. (1999). Detecting action potentials in neuronal populations with calcium imaging. Methods *18*, 215–221.

Stocker, R.F., Lienhard, M.C., Borst, A., and Fischbach, K.F. (1990). Neuronal architecture of the antennal lobe in *Drosophila melanogaster*. Cell Tissue Res. *262*, 9–34.

Tanaka, N.K., Awasaki, T., Shimada, T., and Ito, K. (2004). Integration of chemosensory pathways in the *Drosophila* second-order olfactory centers. Curr. Biol. *14*, 449–457.

Tanaka, N.K., Tanimoto, H., and Ito, K. (2008). Neuronal assemblies of the *Drosophila* mushroom body. J. Comp. Neurol. *508*, 711–755.

Tanaka, N.K., Endo, K., and Ito, K. (2012). Organization of antennal lobe-associated neurons in adult *Drosophila melanogaster* brain. J. Comp. Neurol. *520*, 4067–4130.

Tasic, B., Menon, V., Nguyen, T.N., Kim, T.K., Jarsky, T., Yao, Z., Levi, B., Gray, L.T., Sorensen, S.A., Dolbeare, T., et al. (2016). Adult mouse cortical cell taxonomy revealed by single cell transcriptomics. Nat. Neurosci. *19*, 335–346.

Trannoy, S., Redt-Clouet, C., Dura, J.M., and Preat, T. (2011). Parallel processing of appetitive short- and long-term memories in *Drosophila*. Curr. Biol. *21*, 1647–1653.

Turner, G.C., Bazhenov, M., and Laurent, G. (2008). Olfactory representations by *Drosophila* mushroom body neurons. J. Neurophysiol. *99*, 734–746.

von Philipsborn, A.C., Liu, T., Yu, J.Y., Masser, C., Bidaye, S.S., and Dickson, B.J. (2011). Neuronal control of *Drosophila* courtship song. Neuron *69*, 509–522.

Wu, C.L., Shih, M.F., Lai, J.S., Yang, H.T., Turner, G.C., Chen, L., and Chiang, A.S. (2011). Heterotypic gap junctions between two neurons in the Drosophila brain are critical for memory. Curr. Biol. *21*, 848–854.

Wu, C.L., Shih, M.F., Lee, P.T., and Chiang, A.S. (2013). An octopamine-mushroom body circuit modulates the formation of anesthesia-resistant memory in *Drosophila*. Curr. Biol. *23*, 2346–2354.

Xie, Z., Huang, C., Ci, B., Wang, L., and Zhong, Y. (2013). Requirement of the combination of mushroom body γ lobe and α/β lobes for the retrieval of both aversive and appetitive early memories in *Drosophila*. Learn. Mem. *20*, 474–481.

Yasuyama, K., Meinertzhagen, I.A., and Schürmann, F.W. (2002). Synaptic organization of the mushroom body calyx in *Drosophila melanogaster*. J. Comp. Neurol. *445*, 211–226.

Yuste, R., and Denk, W. (1995). Dendritic spines as basic functional units of neuronal integration. Nature *375*, 682–684.

STAR★METHODS

KEY RESOURCES TABLE

REAGENT or RESOURCE	SOURCE	IDENTIFIER
Antibodies		
Mouse anti-bruchpilot (nc82)	Developmental Studies Hybridoma Bank	nc82; RRID: AB_2314866
Rat anti-GFP monoclonal	Nacalai tesque	04404-84; RRID: AB_10013361
Rabbit anti-GABA	Sigma	A2052; RRID: AB_477652
Vectashield mounting medium antibody	Vector laboratories	H-1000; RRID: AB_2336789
Goat anti-rat IgG (H+L), CF488A conjugated	Biotium	20023; RRID: AB_10557403
Goat anti-mouse IgG (H+L), CF633 conjugated	Biotium	20120; RRID: AB_10556971
Goat anti-rabbit IgG (H+L), CF633 conjugated	Biotium	20122; RRID: AB_10559042
Chemicals, Peptides, and Recombinant Proteins		
Picrotoxin	Sigma	P1675
CGP54626	Tocris	1088
All-*trans* retinal	Toronto research chemicals	R240000
Tetrodotoxin	Tocris	1078
Alexa Fluor 594	Invitrogen	A10438
CF555 streptavidin conjugates	Biotium	29038
Acetylcholine chloride	Sigma	A6625
Mineral oil	Nacalai tesque	23334-85
Ethyl butyrate	Sigma	E15701
Experimental Models: Organisms/Strains		
Drosophila, VT33006-Gal4 in *attP2*	Vienna Drosophila Resource Center	VDRC: 202281; RRID: FlyBase_FBst0486715
Drosophila, VT43924-Gal4 in *attP2*	Gift from A. Chiang, Wu et al., 2013	N/A
Drosophila, APL-Gal4	Gift from A. Chiang, Wu et al., 2013	N/A
Drosophila, Mz19-Gal4	Bloomington Drosophila Stock Center	RRID: BDSC_34497
Drosophila, OK107-Gal4	Gift from K. Ito, Connolly et al., 1996	N/A
Drosophila, UAS-ReaChR::Citrine in *attP40*	Bloomington Drosophila Stock Center	RRID: BDSC_53741
Drosophila, UAS-mCD8::GFP in *attP40*	Bloomington Drosophila Stock Center	RRID: BDSC_32186
Drosophila, UAS-myr::GFP in *attP40*	Bloomington Drosophila Stock Center	RRID: BDSC_32198
Drosophila, UAS-myr::GFP in *attP2*	Bloomington Drosophila Stock Center	RRID: BDSC_32197
Drosophila, UAS-CsChrimson::mVenus in *attP40*	Bloomington Drosophila Stock Center	RRID: BDSC_55135
Drosophila, UAS-GCaMP5G in *attP40*	Gift from V. Jayaraman, Akerboom et al., 2012	N/A
Drosophila, UAS-GCaMP6s in *attP40*	Bloomington Drosophila Stock Center	RRID: BDSC_42746
Drosophila, UAS-GCaMP6s in *VK00005*	Bloomington Drosophila Stock Center	RRID: BDSC_42749
Drosophila, UAS-Archaerhodopsin-3::GFP in *attP40*	This paper	N/A
Recombinant DNA		
FCK-Arch-GFP	Addgene, Chow et al., 2010	22217
pUASTattB	Gift from A.W. Moore, Bischof et al., 2007	FlyBase ID: FBmc0003002

(*Continued on next page*)

Continued

REAGENT or RESOURCE	SOURCE	IDENTIFIER
Software and Algorithms		
Igor Pro	Wavemetrics (https://www.wavemetrics.com/)	RRID: SCR_000325
ImageJ	NIH (https://imagej.nih.gov/ij/)	RRID: SCR_003070
R	R-project (https://www.r-project.org/)	RRID: SCR_001905
MATLAB	Mathworks (http://www.mathworks.com/)	RRID: SCR_001622
Other		
GLUture (surgical glue)	Abbott	N/A
Single channel heater controller	Warner instruments	TC-324B
Thin-wall glass capillary	World precision instruments	TW150F-3
Thick-wall glass capillary	World precision instruments	1B150F-3
Pneumatic picopump	World precision instruments	PV820
Iontophoresis unit	World precision instruments	Model 260

CONTACT FOR REAGENT AND RESOURCE SHARING

Further information and requests for resources and reagents should be directed and will be fulfilled by the Lead Contact, Hokto Kazama (hokto_kazama@brain.riken.jp).

EXPERIMENTAL MODEL AND SUBJECT DETAILS

Flies

Flies were raised on standard cornmeal agar under a 12 hr light/ 12 hr dark cycle at 25°C, except for the flies expressing optogenetic probes, which were raised on the food containing all-*trans* retinal (Toronto Research Chemicals) and kept in dark prior to the experiments. Electrophysiological or imaging experiments were performed on adult females, 3 days or 7-10 days post eclosion, respectively. The following stocks were used: *VT33006-Gal4 (attP2)* (von Philipsborn et al., 2011); *VT43924-Gal4 (attP2) and APL-Gal4 (VT43924-Gal4 (attP2), UAS-Gal4)* (Wu et al., 2013); *Mz19-Gal4* (Ito et al., 1998; Tanaka et al., 2004), *OK107-Gal4* (Connolly et al., 1996), *UAS-ReaChR::Citrine (attP40)* (Inagaki et al., 2014), *UAS-mCD8::GFP (attP40)* (Lee and Luo, 1999), *UAS-myr::GFP (attP40), UAS-myr::GFP (attP2)* (Pfeiffer et al., 2010), *UAS-CsChrimson::mVenus (attP40)* (Klapoetke et al., 2014), *UAS-GCaMP5G (attP40)* (Akerboom et al., 2012), *UAS-GCaMP6s (attP40)* and *UAS-GCaMP6s (VK00005)* (Chen et al., 2013). We generated *UAS-Archaerhodopsin-3::GFP (attP40)* by cloning *archaerhodopsin-3::GFP* (Chow et al., 2010) (Addgene plasmid #22217) into pUASTattB (Bischof et al., 2007) and injecting this plasmid to embryos through a service provided by Genetic Services. The construct was inserted into attP40 site using the ϕC31 integration system (Bischof et al., 2007). Detailed genotypes of flies used in this study are listed in Table S2.

METHOD DETAILS

Electrophysiology

Flies were dissected in the external saline containing (in mM) 103 NaCl, 3 KCl, 5 N-Tris(hydroxymethyl) methyl-2-aminoethanesulfonic acid (TES), 8 trehalose dehydrate, 10 glucose, 26 $NaHCO_3$, 1 $NaH_2PO_4 \cdot H_2O$, 1.5 $CaCl_2 \cdot 2H_2O$, 4 $MgCl_2 \cdot 6H_2O$ (pH ~7.2, osmolarity adjusted to ~275 mOsm). The entire brain was removed from the head capsule and fixed dorsal side up on a glass slide with surgical glue (GLUture, Abbott). The preparation was continuously perfused with the external saline, bubbled with 95% O_2 /5% CO_2 (pH ~7.3). All the experiments were conducted at room temperature (~25°C), and particularly for the experiments in Figure 1, the temperature of the bath was monitored and adjusted to 24-25°C (TC-324B, Warner Instruments). Electrophysiological recordings were made with a Multiclamp 700B amplifier (Molecular Devices) equipped with a CV-7B headstage. Signals were low-pass filtered at 1 kHz and digitized at 10 kHz. Voltages were uncorrected for the liquid junction potential.

PN recordings

Whole-cell patch-clamp recordings from PN somata were performed as previously described (Kazama and Wilson, 2009). In brief, a patch pipette was pulled from a thin-wall glass capillary (1.5 mm o.d./ 1.12 mm i.d., TW150F-3, World Precision Instruments). Resistance of the pipette was typically 8-10 MΩ. The internal solution contained (in mM) 140 KOH, 140 aspartic acid, 10 HEPES, 1 EGTA, 4 MgATP, 0.5 Na_3GTP, 1 KCl, and 13 biocytin hydrazide (pH ~7.2, osmolarity adjusted to ~265 mOsm). Cells were held at around −60 mV by injecting a hyperpolarizing current. GABA receptor antagonists, PTX (P1675, Sigma) and CGP54626 (1088,

Tocris), were dissolved in the external saline at 5 μM and 10 μM, respectively. Cell-attached recordings from PN somata were conducted in a voltage-clamp mode using pipettes filled with external saline. The command potential was adjusted so that the amplifier did not pass any current. To achieve a proper cell-attached configuration, we applied low intensity light from a 594 nm continuous wave laser to induce spikes in PNs expressing ReaChR and adjusted the negative pressure applied inside the pipette until the signal-to-noise ratio of spikes became sufficiently high. Recordings were made from one neuron per brain. After the recording, the brain was gently released from the glass slide and was fixed in 4% paraformaldehyde for > 90 min on ice for immunohistochemistry (see below).

KC recordings

Whole-cell patch-clamp recordings from KC somata were performed with the same procedure as PN recordings with several modifications. A thick-wall glass capillary (1.5 mm o.d./ 0.84 mm i.d., 1B150F-3, World Precision Instruments) was pulled and pressure-polished (Goodman and Lockery, 2000; Johnson et al., 2008) with a microforge (MF-820, Narishige) and a pneumatic picopump (PV820, World Precision Instruments). The air pressure was adjusted to ~35 psi. The final pipette resistance was typically 10-12 MΩ. Cells were held at around −60 mV by injecting a hyperpolarizing current unless otherwise mentioned. To assess the quality of KC recordings during experiments, we injected current steps at several separate times, and aborted the recording if the KC did not spike in response to the stimulation. In Figure 2, all the physiological properties were measured shortly after attaining the whole-cell configuration. Tetrodotoxin (1078, Tocris) was dissolved in the external saline at 1 μM. To examine whether *Mz19-Gal4*-positive PNs are connected to the recorded KC or not (Figure 3), KC claws were visualized as previously reported (Gruntman and Turner, 2013). Briefly, Alexa 594 (A10438, Invitrogen) was dissolved in the internal solution at 250 μM and injected into the KC neurites through a patch pipette during recording. After the recording, the brain was immediately fixed in 4% paraformaldehyde at room temperature for a short period of time (10 min) to avoid the attenuation of signals of the dye and the fluorescence of a Citrine protein tagged to ReaChR. The MB calyx was imaged from the posterior side of the brain to obtain clear images of claws with a confocal microscope (Leica TCS SP2) equipped with a 63x water-immersion objective lens (numerical aperture [NA] 0.90). After taking the images of claws, the brain was immunostained to visualize biocytin as described below.

Immunohistochemistry

The brain was stained with antibodies as previously reported (Badel et al., 2016). The following chemicals were used for primary antibodies: nc82 (Developmental Studies Hybridoma Bank), anti-GFP (04404-84, Nacalai), and anti-GABA (A2052, Sigma). Biocytin was visualized by conjugating with Streptavidin:CF555 (29038, Biotium). Vectashield (H-1000, Vector laboratories) was used as mounting medium. Images of the brain were acquired either with a Leica TCS SP2 confocal microscope equipped with a 20x (NA 0.50) or 63x (NA 0.90) water-immersion objective lens, or with an Olympus FV1000-D confocal microscope equipped with a 60x (NA 1.2) water-immersion objective lens.

Iontophoresis

For iontophoresis of ACh, a sharp glass pipette (~15 MΩ) was filled with 10 mM acetylcholine chloride (A6625, Sigma) dissolved in external saline. ACh was ejected into the MB calyx by a brief (500 ms) positive current pulse using an iontophoresis unit (Model 260, World Precision Instruments).

Stimulation of optogenetic probes

LED/mercury light stimulation

Wide-field optical stimulation was achieved by high power LEDs (M470L2 and M590L3 for ReaChR and CsChrimson, respectively, Thorlabs) or filtered light from a mercury lamp (for Arch). An LED (M470L2) with peak output at wavelength of ~470 nm was used for both the activation of ReaChR and excitation of Citrine tagged to ReaChR. Because ReaChR is sensitive to a broad spectrum of light (Lin et al., 2013), blue light was sufficient to make the PNs expressing ReaChR fire at ~200 Hz (Figure S3A). Light from an LED or a mercury lamp was collimated and delivered to an upright microscope (BX51WI, Olympus) equipped with a 40x water-immersion objective lens (NA 0.80). LED light was pulsated at 80 Hz. Neutral-density filters (U-25ND25 or U-25ND6, Olympus) were used to stimulate the cells at lower intensities. All the reported optical intensity of LED light was measured at the back aperture of the objective lens (S120VC sensor, Thorlabs).

IR stimulation

IR stimulation experiments were performed with a two-photon laser scanning microscope (Leica TCS SP2) equipped with a 20x water-immersion objective lens. A Ti:Sapphire laser (MaiTai eHP, Spectra-Physics) was mode-locked at 960 nm. The beam size of the IR laser was adjusted to underfill the back aperture of the objective lens to make the excited volume dictated by the point-spread function slightly larger than convention (Helmchen and Denk, 2005). The intensity was adjusted to 10 mW at the back aperture. The resolution of scanning was 0.17 μm/pixel and the dwell time was 2.4 μs/pixel.

Prior to IR stimulation, the position of the antennal lobe was determined by imaging the signals from Citrine tagged to ReaChR with a continuous wave laser (514 nm). 6 × 6 ROIs (the size of each ROI is 12 μm x 12 μm) were set to cover the antennal lobe along x- and y- axes. The entire depth of the antennal lobe was covered by scanning 18 frames each separated by 5 μm along the dorsoventral axis (z axis). ROIs were stimulated by an IR laser individually in turn. PNs responded maximally at a certain ROI and much weakly at several of orthogonally located collateral ROIs, forming a "cross" shaped response pattern (Figure S1H). Responses outside of this "cross" region were negligible. Stimulation of neither cell bodies nor the medial antennal lobe tract (axons) evoked action potentials in PNs.

To study how PN inputs are integrated in KCs, we isolated two cross-shaped ROIs to be stimulated that fulfilled the following criteria (Figure S2A). First, they did not overlap with each other along the x- and y-axes. Second, they were located in the same focal plane and that within three rows of ROIs to be stimulated at short intervals. Under this condition, centers of two ROIs were stimulated within 173 ms. The same procedure was applied to examine the integration of input from three ROIs (Figures S2A and S2B). Because of experimental constraints, we could not examine the integration of more than four ROIs.

Calcium imaging

Odor-evoked calcium responses of APL neurons and KCs were recorded *in vivo* with a two-photon laser scanning microscope (LSM 7 MP, Zeiss) equipped with a water-immersion objective lens (W Plan-Apochromat, 20x, NA 1.0) as previously described (Badel et al., 2016) with several modifications. Briefly, individual flies were attached to a custom-made recording plate and a small portion of the head cuticle was removed to expose the MB medial lobes. The external saline added on top of the plate was circulated throughout the experiment. Ethyl butyrate (E15701, Sigma-Aldrich) diluted in mineral oil (23334-85, nacalai tesque) by 5 different factors (10^{-9}, 10^{-7}, 10^{-5}, 10^{-3}, and 10^{-1}) was presented for 1 s at 30 s inter-trial-interval with a custom-made olfactometer (Badel et al., 2016). Ethyl butyrate at each concentration was presented four times (Figures 6 and 8) or ten times (Figure 7) in random order. GCaMP was excited with a Ti:Sapphire pulsed laser (Chameleon Vision II, Coherent) mode-locked at 930 nm. The laser intensity was adjusted to ~16 mW at the back aperture of the objective lens. The scanning resolution was 2.08 μm/pixel and the dwell time was 16.6 μs/pixel (23 ms/frame) for Figures 6 and 8, and 6.52 μs/pixel (9 ms/frame) for Figure 7, respectively. GCaMP signals in β, β′, and γ lobes were analyzed at their tips where different lobes are clearly segregated in space (Figures 6C and 7A) by setting a 16.64 μm x 16.64 μm ROI, which roughly covers the tip. Mean GCaMP fluorescence within a ROI was calculated using ImageJ (NIH). The reported change in fluorescence (ΔF/F) in Figures 6 and 8 is an average of three, fixed frames around the peak response.

QUANTIFICATION AND STATISTICAL ANALYSIS

All statistical analyses were performed in MATLAB or R. Sample sizes were not estimated in advance. Statistical tests, significance, and sample size are reported in the figures and figure legends. All mean values are reported as mean ± SEM. K-means clustering (Figure 3) was performed in R. Onset time of a response in Figure 7D was detected by a previously described algorithm (Kudoh and Taguchi, 2002). Dynamic range in Figure 8D was calculated in each condition (with or without GABA receptor antagonists) by subtracting the response to 10^{-9} from that to 10^{-1} dilution, normalized by the response to 10^{-1} dilution. Note that the dynamic range can be larger than 1 when the response to 10^{-9} dilution is slightly negative.

Linear discriminant analysis (Figure 8) was performed in R with MASS package as described previously (Bhandawat et al., 2007). For each fly and each cell type, data consisted of 20 responses (responses to 4 repeated presentations of odors at 5 different concentrations). We withheld one response from the data and trained the decoder with the remaining 19 responses. After training, we asked the decoder to identify the concentration corresponding to the withheld response. Decoding accuracy shown in Figure 8 represents the average across analyses, each time withholding one of the four responses, for each concentration.